The Journal of Experimental Biology 204, 1333–1345 (2001)
Printed in Great Britain © The Company of Biologists Limited 2001
JEB3203

A STUDY OF HELICAL AND PLANAR WAVES ON SEA URCHIN SPERM FLAGELLA, WITH A THEORY OF HOW THEY ARE GENERATED

D. M. WOOLLEY* AND G. G. VERNON

Department of Physiology, School of Medical Sciences, University of Bristol, University Walk, Bristol BS8 1TD, UK

*e-mail: D.M.Woolley@bristol.ac.uk

Accepted 17 January; published on WWW 15 March 2001

Summary

When the spermatozoon of *Echinus esculentus* swims in sea water containing methyl cellulose (viscosity 1.5–4 Pa s), its flagellum may generate either a helical or a planar waveform, each type being stable. The helical wave, which is dextral, is complicated by the concurrent passage of miniature waves along it. These miniature waves have a pulsatile origin in the neck region of the spermatozoon. Our videotape analysis indicates that there are two pulses of mechanical activity for each true cycle of the helical wave. (The true helical frequency was obtained from the apparent wave frequency and the roll frequency of the sperm head, the latter being detectable in some sperm when lit stroboscopically.) The planar wave has a meander shape. During the propagation of planar waves, the sliding displacements are adjustable in either direction; moribund flagella can undergo unrestricted sliding. The planar waves are, in fact, exactly planar only at interfaces. Otherwise, there tend to be torsions in the interbend segments between planar bends. Mechanical stimulation of the flagellum can cause a sudden transition from the helical to the planar waveform. To account for the two modes of beating, we advance the hypothesis that circumferential linkages yield beyond a threshold strain. Whether this yield point is exceeded, we suggest, depends upon the balance between the active shear force and the external viscosity (among other factors). We propose that a subthreshold force originates in one array and then triggers the other dynein arrays circumferentially, but unidirectionally, around the base of the flagellum; whereas a suprathreshold force provokes bi-directional circumferential triggering. These may be the two patterns of activation that result in helical and planar waveforms, respectively. The transition from helical to planar bending may result from an increment in the force produced by the dynein motors. The pulsatile origin of the helical wave resembles behaviour described previously for spermatozoa of *Ciona intestinalis* and of the quail *Coturnix coturnix*.

Key words: flagellum, spermatozoon, motility, axoneme, dynein, sea urchin, *Echinus esculentus.*

Introduction

In this work, we consider an intriguing question in flagellar physiology, namely, how it comes about that the flagella of some cells generate planar waves while the flagella of other cells generate helical waves. The question is intriguing because the flagellar structure, the 9+2 axoneme, can be essentially the same, as far as one can detect, whatever the waveform.

According to an extensive literature, the flagellar waveform of echinoderm spermatozoa is of the planar type when they swim near a surface (Gray, 1955; Brokaw, 1965; Rikmenspoel, 1978); furthermore, by examining such flagella in side-view, it has been determined that the planarity of the wave is intrinsic rather than imposed by surface forces (Hiramoto and Baba, 1978; Gibbons et al., 1987; Ishijima and Hiramoto, 1994). We have found, however, that by increasing the viscous load on the spermatozoa of *Echinus esculentus*, they can be made to execute helical waves. Much greater increments in external viscosity produce a reversion from helical back to planar bending (although, for accuracy, this wave must be called ‘quasi-planar’). The viscous loads necessary exceed those previously investigated (Brokaw, 1966; Brokaw, 1975; Brokaw, 1996). Abrupt transitions between the two modes of beating can be seen in individual spermatozoa, demonstrating that the distinction between the two modes is entirely functional.

First, we describe briefly the occurrence of the two waveforms. Then, we present a detailed analysis of the helical waveform and show it to be constructed of discrete mechanical pulses. Our numerical analysis indicates that there are two mechanical pulses during each cycle of the true helical wave. Our study of the planar wave is restricted to some unusual features relevant mainly to the ‘sliding microtubule theory’. Finally, we advance a theory suggesting how the standard 9+2 axoneme may generate either type of flagellar wave.

Materials and methods

Sea urchins (*Echinus esculentus* L.) were purchased regularly during June and July from the University Marine Biological Station, Millport, Scotland, and maintained in

Bristol for up to 1 week in an aquarium containing aerated 'Tropic Marin' artificial sea water (ASW) at 10 °C. Spawning was induced by injecting 2–3 ml of 0.5 mol l^{-1} KCl into the perivisceral cavity. Sperm samples were then held on ice, undiluted.

The aim of the work was to observe sperm motility in solutions of very high viscosity. These were 2 % solutions of methyl cellulose (Sigma) in ASW that gave viscosities (nominally) of 0.025, 0.4, 1.5 and 4.0 Pa s according to the molecular mass of the methyl cellulose. In a few trials, we observed sperm diluted in 0.5 mol l^{-1} KCl (no added methyl cellulose). A droplet of one of these solutions was run under a supported coverslip; then a droplet of the sperm suspension was run under so as to interface with the modified ASW. Observations were made, at room temperature (22–24 °C), on sperm that had swum across the interface. A Leitz Ortholux microscope was fitted with an oil-immersion darkfield condenser, and the main data were recorded using a X100 Achromat (with insert stop). In the key experiments, the lamp was a point-source xenon tube (Chadwick-Helmuth Inc., model 8440) synchronized to the 50 Hz unshuttered, interlaced CCD video camera. An ultraviolet barrier filter (Oriel Scientific, no. 59482) was placed below the condenser. All experimental trials were recorded on sVHS videotape, using a Panasonic (AG7350) VCR linked to a For.A video timer (model VTG33F). The system gave a ×5700 magnification on the video monitor.

The analysis of the videotapes was performed manually, 'off-screen', to record positions and wave geometries and, by repeated slow-motion replays, to follow the frequencies visually. For the typical analysis of a spermatozoon with a helical flagellar wave, a sequence was chosen that allowed three cycles of the apparent helical wave (defined below) to be timed. Data for other waveform frequencies and for the velocity of progressive spermatozoa were recorded over this same time interval. Images to represent the typical flagellar geometry were also chosen from within this time interval. In the analysis, each spermatozoon is represented by one such data set.

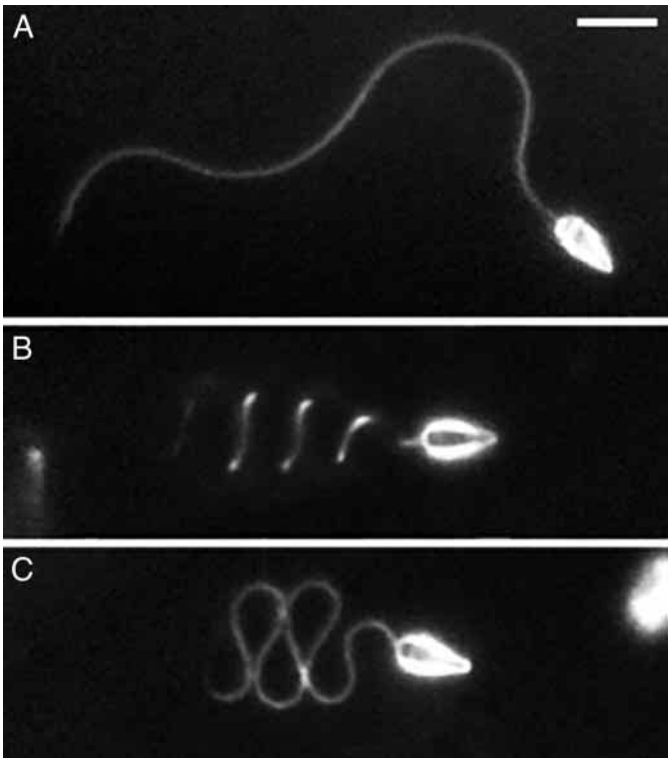

Fig. 1. (A) A spermatozoon swimming against the coverslip in normal artificial sea water (ASW). (B) A helical waveform recorded in ASW of viscosity 1.5 Pa s. The 'bottom' of the helix is in focus, showing that the chirality is dextral. Miniature waves can be detected on the flagellar helix. (C) A planar, meander waveform recorded close to the coverslip in ASW of viscosity 4 Pa s. Video-images, darkfield, stroboscopic illumination. Scale bar, 5 μm.

Results

The general effects of increasing viscosity

The spermatozoa of *Echinus esculentus* are typical for the Echinoidea, with the standard ultrastructure (Afzelius, 1955; D. M. Woolley and G. G. Vernon, unpublished results). We have confirmed observations made long ago that the spermatozoa of this species, when swimming in ordinary sea water (viscosity nominally 1 mPa s), close to a coverslip, move in circular paths, usually clockwise (Buller, 1902); we have seen also that the wave on the flagellum (length 42 μm) is planar, the beat frequency is approximately 50 Hz and the swimming velocity is approximately 200 μm s^{-1} (Rothschild and Swann, 1949). This motility pattern (Fig. 1A) has been well studied in closely related species. We have not analysed it further.

When the external viscosity was raised to 0.025 Pa s, the waveform was usually of the same general type, but the bend amplitude was reduced on the distal flagellum and the swimming velocity was reduced (not illustrated). A detailed study has not been attempted. When the viscosity was raised to 0.4 Pa s, most of the waveforms were no longer planar. Some were regularly helical (as described below), but more typically they were complex, unstable and too difficult to study.

We have based our study on the relatively stable flagellar waveforms seen at two higher viscosities, 1.5 Pa s and 4 Pa s. The essential, surprising finding was that at 1.5 Pa s the flagellar wave was predominantly helical (Fig. 1B), whereas at 4 Pa s it was predominantly planar (Fig. 1C). We have not tried to record the proportionate incidence of these two, quite distinct, waveforms in a quantitative way because (i) the proportions seemed to vary between the sperm samples, and (ii) there was no easy way to assess whether the ratio between the two waveforms might be changing with time.

The helical wave

Description as a simple helix

The helical wave had complicating features that will be considered shortly. However, to begin with, the wave will be treated simply, as being helical in a gross sense. Before

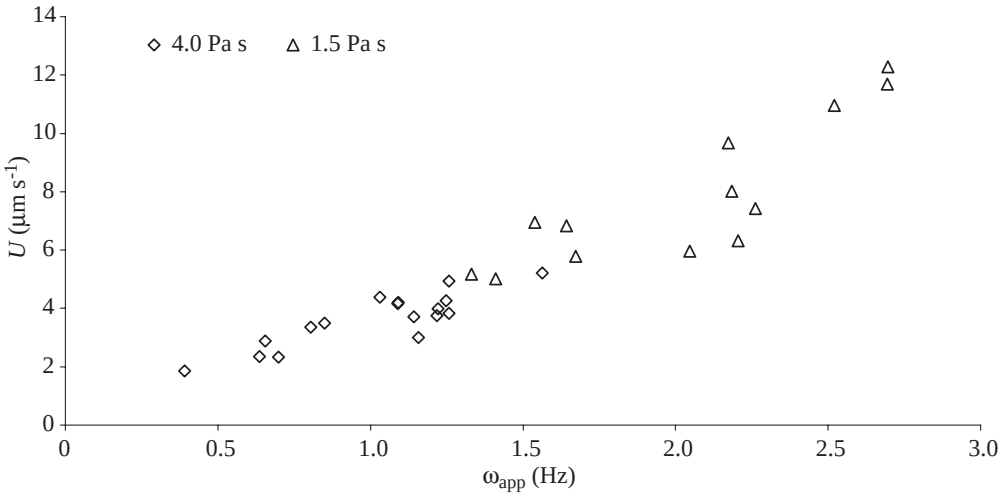

Fig. 2. The relationship between the apparent frequency of the helical wave, ω_{app}, and the forward swimming velocity, U, at two viscosities. The correlation coefficient (pooled data) was 0.94 ($P \ll 0.001$).

presenting the geometrical and dynamic features of this gross helical wave, some well-established theory and notation will be summarized. For helical waves, every element of the flagellum moves in a circular direction about the axis of the helix (the axis that passes through the sperm head) with an angular velocity denoted by ω, the 'true' circular frequency of the flagellar wave. The reaction from the fluid to the torque exerted by the flagellum causes the whole cell to roll (or spin) in the opposite direction, with angular velocity Ω. Because of the drag experienced by the inert sperm head, Ω has a value numerically less than that of ω. Therefore, in the presence of a sperm head, the outcome is that a helical wave is seen to propagate along the flagellum. It has the same chirality as the 'true' flagellar wave, but it has a lower angular velocity, the 'apparent angular velocity' ω_{app}, given by ω–Ω. Forward propulsion is due to the thrust elicited by the apparent helical wave. For a formal hydromechanical analysis of this phenomenon and the earlier literature, see Chwang and Wu (Chwang and Wu, 1971).

In *Echinus esculentus*, the gross helix held slightly fewer than three cycles of bending (Fig. 1B). In fact, the wave amplitude grew on the proximal flagellum and was then maintained; the gross geometry was thus conical at first, becoming helical. As determined by differential focusing, the helix was, without exception, dextral. This means that each element of the flagellum was moving anticlockwise (as would be seen from a forward viewpoint); indeed, occasional views of sperm swimming downwards from the plane of focus showed the flagellar tip following a helical path clockwise from this rear viewpoint. The amplitude and wavelength (Table 1) were not significantly changed by raising the viscosity from 1.5 to 4 Pa s.

The apparent angular velocity of the gross helical wave (ω_{app}) was easily estimated. It was significantly reduced at the higher of the two viscosities (Table 1). The forward velocity of the spermatozoon, U, was closely correlated with ω_{app} (Fig. 2, statistics are given in the legend). The swimming trajectory of the helices was usually exactly straight, but they would follow a circular path (always clockwise) when very close to the coverslip. An extreme example of this motion is shown in Fig. 3.

To discover the 'true' angular velocity of the flagellar wave, ω, one needs to estimate the angular velocity of the roll of the whole cell, Ω, as well as ω_{app}. This was achieved by closely observing the sperm head, which, although essentially pyriform and symmetrical, in some cases had a slight asymmetry (Fig. 4A) and in others contained small particulate features that acted as self-luminous points in darkfield illumination (Fig. 4B). In slow-motion replay, either type of irregularity could be followed visually to give an estimate of Ω. (The direction of the roll could not be detected, nor could we rule out the possibility of a strict 180° angular oscillation but, from the theory outlined above, a continuous clockwise roll is assumed.) For the progressively swimming spermatozoa, the estimates of ω_{app} and Ω are given graphically (Fig. 5); there was a significant correlation between these two variables (see legend to Fig. 5). From the gradient of the fitted slope, the average value for ω_{app}/Ω is 0.2; this gives ω/Ω=1.2, on the basis of the assumption made above. The derived variable ω will be considered below.

In principle, a 'true' flagellar angular velocity, ω, should be displayed by a cell if it becomes fortuitously attached to the slide or coverslip by the head, at which time the rolling of the

Table 1. *Characteristics of helically swimming spermatozoa at external viscosities of 4 and 1.5 Pa s*

External viscosity (Pa s)	ω_{app} (Hz)	U (μm s^{-1})	a (μm)	λ (μm)
4 (N=17)	1.02±0.30	3.63±0.92	3.10±0.24	4.00±0.69
1.5 (N=13)	2.03±0.47*	7.85±2.50*	2.88±0.41	4.66±0.66

Values are means ± S.D. for the apparent angular velocity of the helical wave (ω_{app}), the forward swimming velocity of the spermatozoon (U) and the amplitude (a) and wavelength (λ) of the gross helical wave.

An asterisk indicates a significant difference between the two viscosities (P<0.001; Student's t-test).

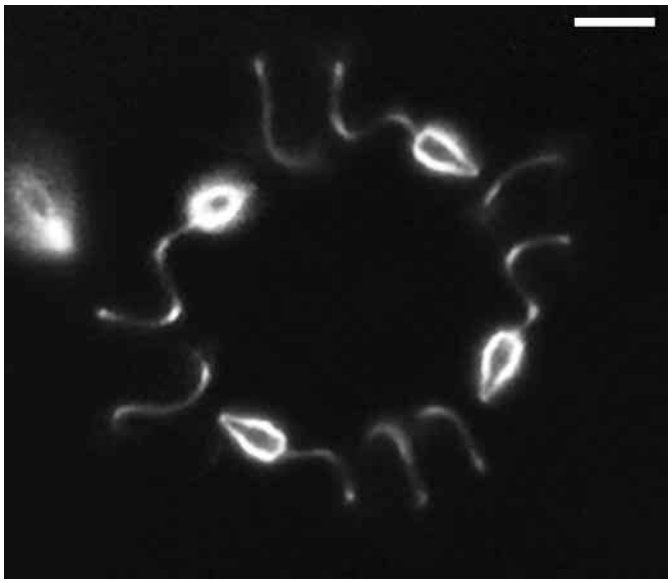

Fig. 3. A montage of four video images of a single spermatozoon to demonstrate that spermatozoa executing helical waves can follow circular paths. Intervals between frames are approximately 2 s. Scale bar, 5 μm.

cell might be expected suddenly to cease. We recorded 10 instances of cells that were swimming as helices, progressively, and then became stuck but continued without interruption to generate helical waves. The wave was compressed in this condition (Fig. 6). To our initial surprise, the observed angular velocity of the helical wave after attachment did not increase: in five cases, it was reduced and in five cases unchanged. The explanation is that the attachment of the sperm head to the coverslip did not, in fact, prevent the rolling of the cell as we had expected. Instead, the contents of the head continued to roll within the membrane, as detected by the rhythmic motion of the irregular head features described above. Indeed, because of the confinement of the head, the roll frequency for attached sperm was easier to appreciate than in free-swimming cells. In addition to the 10 sperm recorded in the process of becoming attached, many more were found already attached, and recordings from this large set provided further important data (see below).

Description of complicating features

We had recognized immediately that the gross helical shape of the flagellum always had, superimposed on it, a train of small-scale waves (Figs 1B, 3, 4, 6). Also, the whole flagellum appeared to vibrate. The origin of these small waves was in the most proximal part (the neck region) of the flagellum. The anticlockwise sweep that was generating the gross helical wave was not smoothly continuous but consisted of a rhythmic succession of accelerations and decelerations. We refer to these as 'pulses' of mechanical activity. They had two effects: they set up a train of small-scale bends on the flagellum that persisted and even seemed to grow in amplitude distally, and, with each 'pulse', the whole flagellum was momentarily drawn

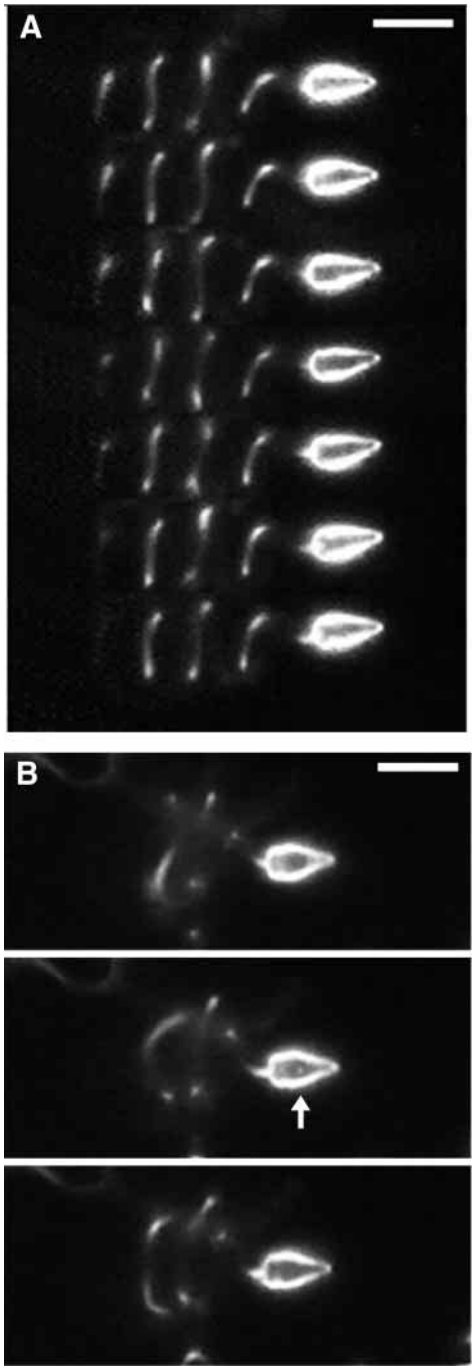

Fig. 4 (A) A montage of seven video images of a single spermatozoon to demonstrate that it was sometimes possible to detect angular displacement of the sperm head about its own longitudinal axis. Intervals between frames are each 20 ms in the downward direction. It may be apparent to the viewer that the image of the head is varying in detail, with the top and bottom images being most similar. These images also demonstrate how the miniature waves complicate the overall helical shape of the flagellum. Scale bar, 5 μm. (B) A sequence of three video frames of a single spermatozoon that had become attached to the coverslip by its head. The contents of the head continued to rotate, as shown by the transit of bright particulate matter (arrowed). Scale bar, 5 μm.

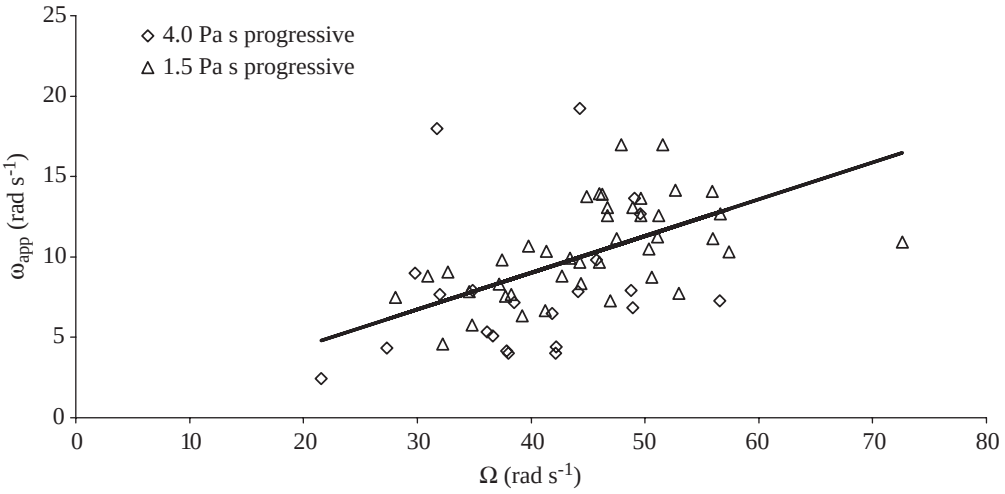

Fig. 5. The relationship between the observed apparent angular velocity of the helical wave (ω_{app}) and the observed angular velocity of the counter-rotation of the whole cell (Ω). Only data for progressively swimming spermatozoa are included. The correlation coefficient (pooled data) was 0.47 (P<0.001). The graph has been treated as a bivariate scattergram (Model II regression) and the slope, gradient 0.23, was computed as the major axis of the ellipse (Sokal and Rohlf, 1995) using a computer program by P. Legendre (http://www.fas.umontreal.ca/biol/legendre/).

forward, thus accounting for the vibration of the helix in the direction of its long axis.

Estimates were made of the 'pulse' frequency for the sperm generating helical waves, both for the progressive and for the 'stuck' specimens. In fact, the pulsatility in the neck region was accentuated in those specimens that had the sperm head attached to the coverslip. It was decided that the meaning of the pulsatile behaviour might best be explored by relating the pulsation rate (frequency) to the angular velocity of the true helical wave ω (obtained as $\omega_{app}+\Omega$ and expressed as a frequency). The two frequencies were highly correlated (Fig. 7 and see legend). From the gradient of the fitted slope, the mean value for pulsation-rate/true helical wave frequency was 1.91. We regard this as indicating that each cycle of the true helical wave was associated with two pulses of mechanical activity in the neck of the spermatozoon.

Planar waves

The planar wave (Fig. 1C), the waveform that was predominant in the most viscous medium (4 Pa s), resembled a meander wave (Silvester and Holwill, 1972). The angle of the developed bends was approximately 4 rad. In most cases, there was an asymmetry in bend angle, consistent over time, giving circular swimming paths at the interface with the coverslip; some of these were clockwise and others anticlockwise.

Fig. 6. A sperm shown attached to the coverslip by its head, maintaining a helical wave of compressed wavelength. The mechanical pulsation in the neck region of such specimens was exaggerated and more easily detected than in progressively motile sperm. Viscosity, 1.5 Pa s. Scale bar, 5 μm.

Table 2 presents sample data for beat frequency, forward swimming velocity, amplitude and wavelength at 4 Pa s and 1.5 Pa s. At the lower of these two viscosities, the beat frequency and swimming velocity were greater, with no significant change in bend geometry. At 4 Pa s, beat frequency and swimming velocity were positively correlated (P<0.001); at 1.5 Pa s, there was a smaller range of beat frequency and the correlation coefficient did not reach the 5% level of significance. When planar-swimming sperm became attached by their head to the coverslip, wave compression rapidly followed, and the beat frequency fell (Fig. 8). For five examples at a viscosity of 4 Pa s, the fall in beat frequency was to 52±20% (mean ± S.D.) of the value just prior to attachment. The corresponding increase in bend angle approached 1 rad.

We draw attention to three further, separate patterns of behaviour that may be helpful in understanding the mechanism of the planar waveform and its generation.

Bend loss during propagation

As a prelude to this section, we note that a very tenuous, thread-like extension of plasma membrane was often seen trailing from the tip of the flagellum when the sperm swam, in whichever mode, in the viscous media. These were most common in the medium of viscosity 1.5 Pa s. The longest thread seen was 140 μm. For sperm of other animals, threads

Table 2. *Characteristics of planar swimming spermatozoa at external viscosities of 4 and 1.5 Pa s*

External viscosity (Pa s)	f (Hz)	U (μm s^{-1})	a (μm)	λ (μm)
4 (N=10)	2.81±0.68	9.94±3.44	4.54±0.32	4.11±0.52
1.5 (N=10)	3.80±0.20*	14.89±1.33*	4.52±0.17	4.38±0.45

Values are means ± S.D. for the beat frequency (f), the forward swimming velocity of the spermatozoon (U), the amplitude (a) and wavelength (λ) of the planar wave.

An asterisk indicates a significant difference between the two viscosities (P<0.001; Student's t-test).

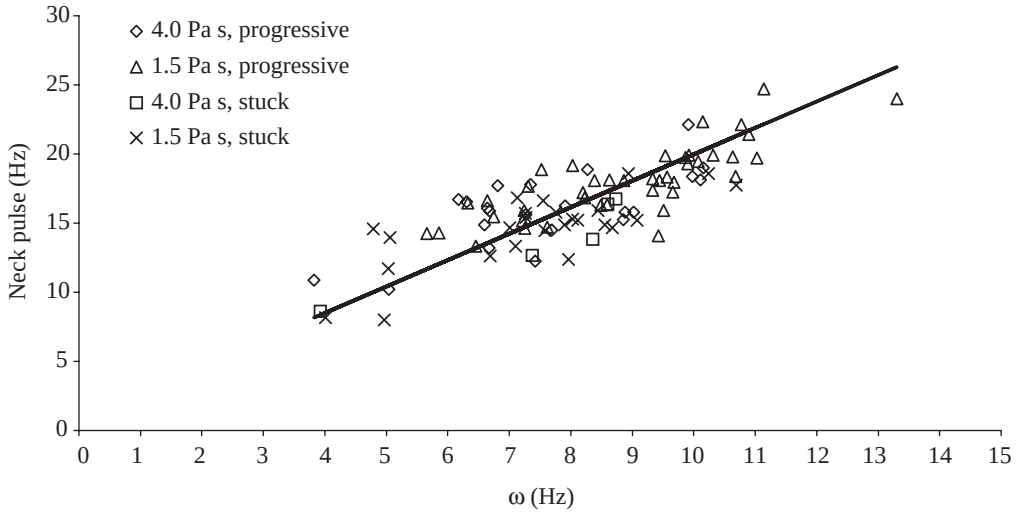

Fig. 7. The relationship between the true angular velocity of the helical wave (ω), derived as ($\omega_{app}+\Omega$, where Ω is the observed angular velocity of the counter-rotation of the whole cell and ω_{app} is the apparent angular velocity of the gross helical wave) and expressed as a frequency, and the observed frequency of mechanical pulsation in the most proximal part of the flagellum (the 'neck pulse'). Data for both progressively swimming and attached (stuck) spermatozoa are included. The correlation coefficient (pooled data) was 0.81 ($P \leqslant 0.001$). Further analysis was as for Fig. 5. The mean values were 8.1 Hz (ω) and 16.4 Hz ('neck pulse'). The gradient of the slope was 1.91 (95 % confidence interval 1.6–2.2).

of this kind have been investigated and pictured in detail (Woolley, 1995). We have not therefore attempted to illustrate them again, even though they have not been reported before for sea urchin sperm. *Echinus esculentus* sperm with long threads commonly showed distortions of the waveforms, presumably because of the drag force experienced by the thread. The typical distortion seen in a small proportion of the planar waveforms was the complete decay of one entire cycle of bending while the other propagating bends maintained their form (Fig. 9). This occurred repeatedly, with each cycle of bending.

Deformation due to agonal sliding

We noticed that spermatozoa that had entered the viscous medium and had then become attached to the coverslip might appear to have 'branched' flagella. This is an agonal (*pre-mortem)* deformation, and on one occasion it was recorded as it happened. It began with a local rupture of the axoneme and a looping-out of part of it, then a twisting of the loop (possibly by 180 °), and the loop then growing in length upon itself in the manner of a hairpin. As the loop grew in length, the axoneme distal to the loop reduced its thickness (brightness) progressively from the tip (Fig. 10). Thus, the looped segment finally reached half the length of the axoneme remaining distal to it. In this specimen, the rate of loop-elongation was constant at 1.1 μm s^{-1}, half the rate at which the full-brightness segment of the distal flagellum reduced its extent (Fig. 11). Prior to becoming disrupted, this sperm had been swimming normally

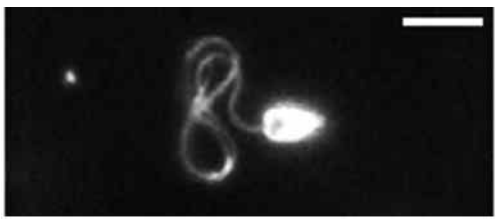

Fig. 8. A sperm shown attached to the coverslip by its head, maintaining a planar wave of compressed wavelength. Viscosity, 4 Pa s. Scale bar, 5 μm.

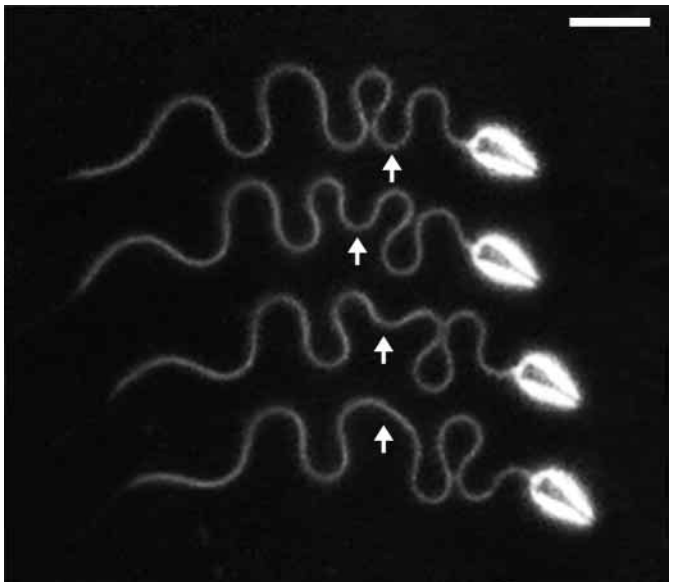

Fig. 9. A montage of four video images of a single spermatozoon, showing the loss of one cycle of bending (arrowed) during propagation. The spermatozoon was trailing a thread of membrane from the tip of its flagellum (not visible). Intervals between frames are 0.24 s, 0.08 s and 0.12 s in the downward direction. Scale bar, 5 μm.

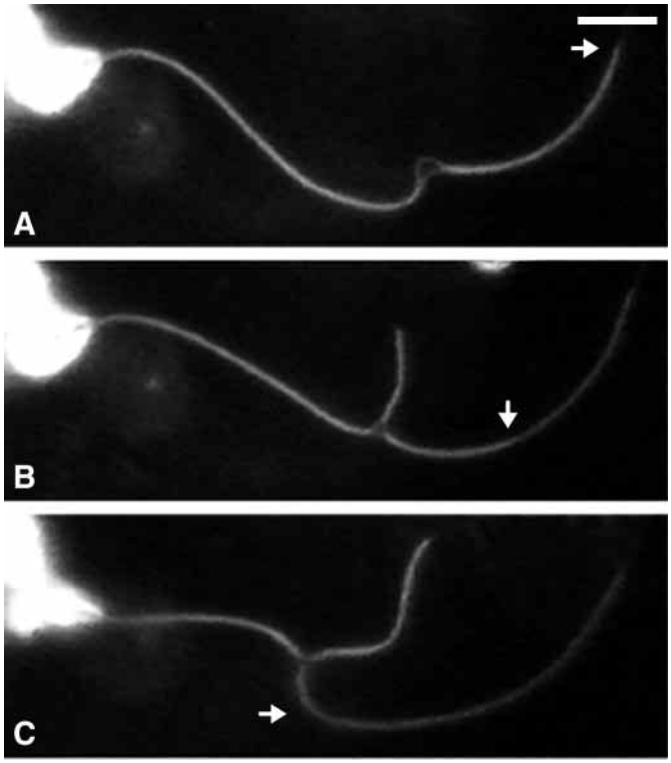

Fig. 10. A set of three video images (A–C) of a single spermatozoon, showing the example of agonal sliding discussed in the text, with measurements given graphically in Fig. 11. The arrow in each image locates the position where there is a step-change in the brightness of the distal flagellum. Intervals between frames are 6.28 s and 5.82 s in the downward direction. For clarity, an extraneous cell had been removed from this figure electronically. Scale bar, 5 μm.

(beat frequency 2.0 Hz; bend angle, 4 rad), except for having a flexure of 180° at the neck. Sperm could survive this disruption in the sense that the flagellum proximal to the loop, in some cases, kept beating in the planar mode. Examples of multiple loops were found.

Loss of overall waveform-planarity

Because of the slow swimming speeds imposed by the viscous media (1.5 Pa s and 4 Pa s), it was possible to observe planar swimming of spermatozoa far from the coverslip. Such swimming was easily recognised as planar rather than helical because the sperm flagellum showed meander-type waves, the spermatozoa swam at the characteristically higher velocity and the flagellar movement became truly planar when they did reach the coverslip. However, away from the surface, the waveform as a whole was not planar. At this point, it should be noted that a planar wave has been regarded analytically as a sequence of bends (arcs) separated by interbend regions or interbends (straight) (see Brokaw, 1965). Even though a meander wave is analytically distinct from this (Silvester and Holwill, 1972), we shall nevertheless use the 'bend/interbend' terminology as a convenient way to describe the deviation from planarity when the sperm of *Echinus esculentus* were not close to the coverslip. In such situations, only the individual bends of the waveform remained planar, as could be seen in side-views. The waveform as a whole was a succession of planar bends separated by interbend regions that seemed to have undergone torsion. The wave is only quasi-planar. As perhaps the simplest example of a quasi-planar wave, consider the 'loop-the-loop' motion represented in Fig. 12. Alternate bends are in-focus, and these, viewed in profile, appear as straight lines. This waveform can be developed from the truly planar type (Fig. 1C) by imposing localized torsions in each of the interbend regions. A simple wire or paper model will show that these torsions need to have alternating chirality. In fact, the 'loop-the-loop' pattern is probably a special case, being itself stabilised by the proximity of a coverslip. Usually, the loop is not closed and the sperm translates through the fluid along a helical path. This was often seen, but is difficult to demonstrate in micrographs. One sees a quasi-planar waveform following a helical direction; this is quite different from the helical flagellar wave described above. Pending a full analysis of quasi-planar waveforms, at this stage, we merely note the evidence for interbend torsion and the suppression of any such

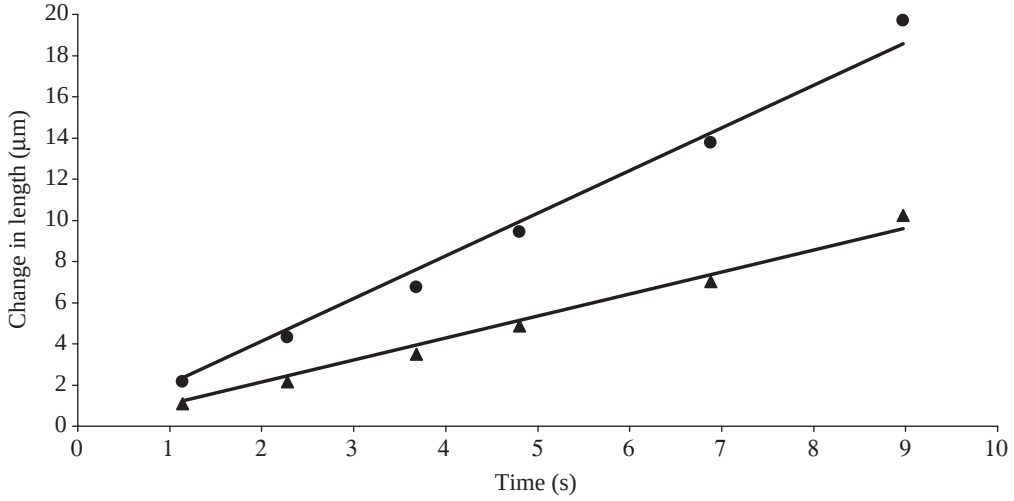

Fig. 11. A quantitative analysis of the event illustrated in Fig. 10. The graph shows the rate of change in the length of the 'branch' extending from the flagellum (▲) and the rate of change in the length of the zone of diminished brightness of the flagellum proper (●) (distal to the arrows in Fig. 10). The velocity of sliding in the flagellum is given by the regression coefficient for the upper plot, 2.1 μm s^{-1}. The branch grows at half this rate because it is doubling on itself.

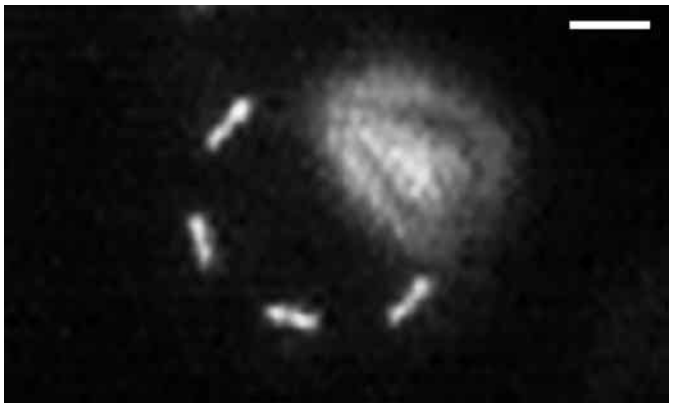

Fig. 12. A spermatozoon swimming close to but not at the interface with the coverslip (viscosity 4 Pa s). This is interpreted as a 'planar' wave (preferably termed quasi-planar) in which torsions have developed in the interbends because the spermatozoon is not swimming at the interface with the coverslip. Scale bar, 5 μm.

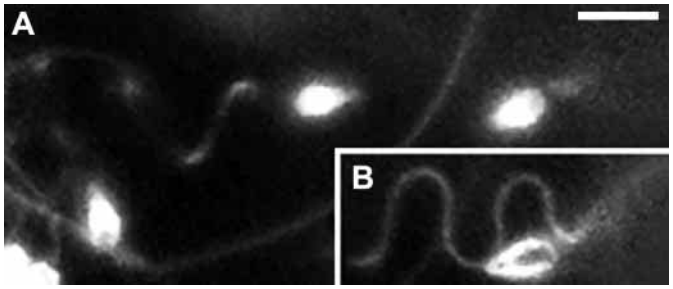

Fig. 13. (A) A spermatozoon executing helical waves but experiencing entanglement (at left). (B) Inset showing the same flagellum having switched to planar beating. The image was captured just before the spermatozoon accelerated out of the field of view. Viscosity, 0.4 Pa s. Scale bar, 5 μm.

torsion when the planar flagellar bends are generated close to and in the plane of an interface.

Sudden transitions between helical and planar waveforms

Sperm that swam with a helical flagellar wave, upon becoming trapped in entanglements of other cells, in some cases suddenly performed a few cycles of planar bending that caused them to accelerate through the obstruction (Fig. 13). Usually, such a sperm would then be lost to view, but a few were seen to resume helical beating. Helical-to-planar switching was seen in media of 0.4, 1.5 and 4 Pa s viscosity (11 examples in all). All, with the possible exception of one, resulted from the encounter of a sperm with an obstruction. It was not necessary for the sperm head to hit the obstruction: contact with the flagellum was sufficient to induce planar beating. Indeed, sperm that became stuck solely by the head did not undergo the helical-to-planar transition (see above). Conversions from planar to helical beating were also witnessed, though less often.

Discussion

Our observations are a development of those made by Brokaw on other invertebrate spermatozoa of the simple 9+2 type (Brokaw, 1966). A reduction in plane-wave amplitude, observed by us using a medium of 0.025 Pa s, was observed by him for the sperm of *Ciona intestinalis* (tunicate) and *Lytechinus pictus* (Echinoidea) in a series of viscosities up to 0.1 Pa s. A large increase in planar-wave bend angle, observed by us using media of 1.5 Pa s and 4 Pa s, was described by him for the sperm of *Chaetopterus variopedatus* (Annelida) in a series of viscosities up to 0.94 Pa s and for *Lytechinus pictus* sperm moving with lowered beat frequency. Compression of plane waves following attachment of the sperm head to a glass surface is also well known (Brokaw, 1965). In some experiments, Brokaw (Brokaw, 1965) used thiourea to reduce the beat frequency of planar waves. Unexpectedly, when he applied 0.1–0.2 mol l^{-1} thiourea to sperm of *Ciona intestinalis*, swimming in a medium of viscosity 0.008–0.01 Pa s, the flagellum 'forms a helix, generated at rates of 1–2 turns/sec, with a pitch of about 20 μm and a radius of about 6 μm. Both left-handed and right-handed helices are common. In addition, a transverse vibration of small amplitude (1 μm or less?) with a frequency of 10–15/sec is seen, which appears to represent the passage of small-amplitude waves along the flagellum. Since many spermatozoa attached to the slide by their heads show the same propagated helical waves, the swimming … cannot be explained by assuming that the rigid helix is propelled by the small amplitude vibrations.' (Brokaw, 1966). This description clearly conveys the essential features of the helical waves in *Echinus esculentus*.

In the present paper, we have drawn attention primarily to the helical wave, to its incidence and to its complicating features. A helical wave has not been reported previously for sea urchin spermatozoa. It now seems that it is one of two stable waveforms achievable by the standard 9+2 axoneme. The probability of a helical wave being generated is affected by changing the external conditions (viscosity) and also, presumably, by a change in intracellular conditions consequent on a collision. A general explanation of these facts will be attempted, following some detailed discussion of our findings.

The interpretation of the helical wave

The flagellar helix is a continuously generated wave. If it were a rigid helix propelled by vibrations, it would not be possible for the head to roll at a higher frequency than the 'apparent wave frequency'. The grossly helical wave should thus conform to the basic principle of helical waves, even though the circular movement that generates the helix is not a smooth displacement. The principle, already briefly explained, is that the apparent angular velocity is the sum of the circular frequency of the flagellar wave and the angular velocity of the sperm ($\omega_{app}=\omega+\Omega$). From the work of Chwang and Wu (Chwang and Wu, 1971), the value of ω/Ω at equilibrium is constant for sperm of given dimensions executing waves of given wavelength and amplitude, and the value is independent

of external viscosity. Where ω/Ω is constant, then a direct proportionality is to be expected between ω_{app} and Ω, the measurable angular velocities. The correlation obtained (see Fig. 5) was rather weak, although highly significant. The problems with this approach are the difficulty of determining Ω, variability in wavelength and amplitude, and the likelihood of viscous interaction with the coverslip. (This interaction is significant in that it is thought to account for the circular swimming of helices near the coverslip; M. E. J. Holwill, personal communication.) Nevertheless, the average value we obtained for ω/Ω, 1.2, is reasonably similar to the value of 1.1 that we have calculated from the theoretical work of Chwang and Wu (Chwang and Wu, 1970), using their equation 36, approximating the sperm head as a sphere of radius 1.3 μm, and taking the wavelength (λ) and amplitude (a) from Table 1. In view of this relationship between ω and Ω, and because of the close correlation between ω_{app} and U, we believe that the motility is conforming to the normal principles of helical waves.

This being accepted, the estimate of ω for each sperm will have validity. This parameter is important as being the rate at which the mechanical process is moving around the axonemal cylinder. We have used it to try to explain the basis of the pulsatility in the generation of the helix and concluded, on the basis of the analysis of the data in Fig. 7, that the pulse frequency is twice the true wave frequency. This generalisation is put forward, in spite of the variability (see Fig. 7), which may have arisen because the pulse frequency was difficult to determine. In addition, the estimates of ω incorporated errors associated with the difficult visual estimation of Ω.

It is not clear why two pulses of mechanical activity should be found with each cycle of the flagellar wave. However, we favour the interpretation that the two pulses are really a double-pulse, because this interpretation is consistent with our recent observations on the 9+2 axonemes of quail spermatozoa (Woolley and Vernon, 1999). In quail spermatozoa, at very high viscosities, double mechanical pulses were seen, each involving 180° torsions of the axoneme. Our provisional interpretation of the double-pulse, applicable to both situations, is that one pulse is active and generates torsion (with shortening), whereas the other pulse, running ahead, represents a passively imposed reverse-torsion and shortening (see Woolley and Vernon, 1999).

Deformations of the planar waves

Compression of the wave upon sticking by the head and bend loss during propagation

According to the geometrical theory for symmetrical planar waves without torsion, the bend crests are regions of zero sliding displacement and maximal instantaneous sliding velocity; the mid-interbend region, in contrast, is the region of maximal sliding displacement and zero instantaneous sliding velocity (Gibbons, 1982). It is of interest that, when a waveform is stretched by the drag force on a terminal thread of membrane, and a bend decays as it propagates, then the underlying, necessary sliding readjustment is a reversal of the sliding that had been established in that cycle, which is presumably the cycle subjected to the greatest stretching force. Similarly, when the propagating waveform is compressed (following head attachment) rather than stretched, the sliding readjustment is an extension of sliding in the same direction as that already established. For the compressed waves (Fig. 6), the maximum sliding displacement (between doublets 3 and 4) will be approximately 0.25 μm. In both cases, the modulation of the degree of sliding will be occurring in the segments between the bend crests, i.e. in segments where there is already some sliding displacement. In an analogous situation, localised wave compression and expansion can be induced by holding the sperm head on a suction micropipette and imposing a vibration axially with respect to the head axis (Shingyoji et al., 1991a). By that method, stretching the wave caused a reduction in bend angle in proximal but not distal bends; whether this was due to passive sliding or elastic distortion was uncertain. In the phenomenon of bend loss (Fig. 9), it is noteworthy that only one discrete cycle of bending was affected, and totally eliminated; the other, adjacent cycles were not stretched. For a flagellum that is developing forward thrust yet experiencing drag from a passive tip-thread, we suggest that the stretching force will be greatest in mid-flagellum, and it is here, therefore, that its magnitude is most likely to exceed the active bending moment. When it does, as soon as the sliding begins to be reversed (beginning of bend loss), the stretching force on adjacent bends will be immediately lessened.

Agonal sliding

Rupture of the axoneme and the sliding out of a tightly opposed loop was not a rare event, but it was recorded only once from beginning to end. The axoneme behaved as two halves sliding against each other at a constant velocity, $2.1\,\mu m\,s^{-1}$. This sperm had been swimming in planar mode and, from its beat frequency and bend angle, it is calculated that its maximal sliding velocity between doublets 3 and 4, when it was swimming, was $2.7\,\mu m\,s^{-1}$ (using equation 3 of Takahashi et al., 1982). The agonal sliding phenomenon indicates that there can be unlimited sliding at physiological rates in live cells. Whatever resistances exist within the axoneme, they can be overcome by the active force, without the need for the protease treatment that is necessary to permit the unlimited sliding of reactivated flagella. However, internal disruption is needed to show this, and the question of whether the resistances are irreversibly affected by such sliding cannot be examined.

Loss of planarity

In solutions of high viscosity, strictly planar waves were seen only near the coverslip. Away from the coverslip, each bend on the wave was planar, but there was flexibility of the interbend segments. In reaching this conclusion, we began by considering how the wave seen in Fig. 12 might arise, using paper models. We found that interbend torsions of equal magnitude and alternating chirality, between plane bends of π rad (bend angle θ), reproduce this wave, which runs

transversely around a cylindrical surface (the 'loop-the-loop' pattern). More commonly, however, the sperm swam progressively by taking a direction in the cylindrical surface oblique to the long axis. To model this, we considered the more extreme case, i.e. how a wave of this type might conform approximately to a cylindrical surface if it swam parallel to the long axis of the cylinder: this could be achieved by imposing a tilt upon each interbend region, keeping all the bends planar. By interpolation, then, we conclude that conforming to an oblique path involves both torsion and tilting of the interbend segments. (We could not model the helical path by having the bend angle greater or less than π rad, nor by introducing bend asymmetry, nor by having interbend torsions of unequal magnitude.) It is not clear how the chirality of the helical path could be established, and we do not have enough data to determine whether both chiralities actually occur with equal likelihood. Our overall conclusion is that, in a geometrical sense, interbend flexibility can account for the three-dimensional paths taken by quasi-planar waveforms when spermatozoa swim deep into highly viscous solutions. Interbend torsion has been described before, in mammalian spermatozoa (Woolley, 1977; Woolley and Osborn, 1984). Further study of the sea urchin waveforms is needed. A related issue is whether the helical chirality (in a deep chamber) determines the circling direction (at the coverslip), an issue of interest because the latter is influenced by the prevailing Ca^{2+} concentration (Ishijima and Hamaguchi, 1993).

An attempted general explanation

It is evident now that the sea urchin sperm flagellum, the subject of classical analyses of planar waves, can also execute helical waves. How can the '9+2' axoneme switch functionally between helical and planar bending and why is viscosity influential? The likelihood is that some structure within the axoneme can exist in two stable states. Doublet or singlet microtubules themselves have been thought to have this property (Jarosch, 1986; Amos, 1991) but, as will be seen, we have tentatively given this role to the interdoublet (nexin) link.

We offer several hypotheses that together may provide a provisional general theory.

(i) First, we postulate interdoublet links that are elastic only up to a threshold strain, and then yield.

(ii) Second, we say that whether the strain in these links reaches the yield point or not will depend on the balance between the active bending moment and the bending moment due to the external viscosity.

(iii) We now consider events at the base of the axoneme. The third, triple, postulate is that the dynein complexes normally activate spontaneously only at the proximal end of an inter-doublet array, that all subsequent activations are strain-dependent and that, after activation, there is a refractory period.

(iv) Fourth, we imagine the initial activation triggering adjacent arrays circumferentially as well as triggering the same array proximo-distally (metachronally).

(v) Three-dimensional or two-dimensional waves can now arise as a consequence of the threshold behaviour of the interdoublet links. As the fifth proposal, we say that a subthreshold strain can trigger circumferential activation only unidirectionally, thereby generating a cycle of helical bending; but a suprathreshold strain, and the yielding of the interdoublet links, triggers circumferential activation bi-directionally, initiating a cycle of planar bending.

(vi) To explain the reversion to planar bending at extreme viscosity, or following collision, our sixth hypothesis is that an increment of active shear force is possible as a result of some undefined mechanosensitivity of the flagellum.

Some discussion of these hypotheses follows.

(i) In the compressed plane waveform shown in Fig. 8, the maximum inter-doublet displacement is approximately 250 nm, a length equivalent to 10 of the outer dynein arms. This makes it unlikely that any interdoublet linkage could remain attached. The identity of the detachable link is probably the circumferential (or nexin) link first described by Gibbons (Gibbons, 1963), although there are other possibilities. The suggestion that these nexin links can tilt and also yield at their B-end attachment is supported by some electron microscopical studies (Warner, 1983; Bozkurt and Woolley, 1993) and by direct measurements of elasticity (Minoura et al., 1999). The claim that they can functionally detach is supported by the observations of Kamiya and Okagaki (Kamiya and Okagaki, 1986), who reported the separation and re-attachment of flagellar doublets in *Chlamydomonas reinhardtii* between periods of active shear. Our observations on planar waves in moribund sperm of *Echinus esculentus* indicate that the active force in live cells can be sufficient to cause unlimited sliding between doublets. The need, in theoretical treatments of bend-asymmetry, to postulate 'synchronous' sliding throughout actively propagating planar waves (Gibbons, 1982) would seem to require that all the nexins are functionally detached. This concludes the evidence that the nexin links may become detached from the adjacent doublet. We note the evidence that radial spokes may behave in a similar way, detaching from the central structures (Warner and Satir, 1974).

(ii) In principle, the active bending moment (M_A) generated within the axoneme is balanced at each position on the flagellum by the sum of the bending moment due to the external viscosity (M_V) and the bending moment due to the elasticity of structures within the axoneme (and, for some flagella, structures around the axoneme) (M_E). Elastic resistance of the external fluid and viscous resistance within the flagellum are considered negligible in comparison. Thus, $M_A+M_V+M_E=0$ (taken from Brokaw, 1988). For a given active force, the strain in the nexin links as they tilt will depend on their own coefficient of elasticity at forces below the yield point and the resistances to bending, namely the stiffness of the axoneme as a whole and the external viscosity.

(iii) Activation must be initiated at the basal end, given the direction in which waves travel. There are, admittedly, some instances of reverse propagation (see Ishijima et al., 1994), and initiation in mid-flagellum can be induced experimentally (Shingyoji et al., 1977). The idea of refractoriness is implicit in the idea of a propagating 'packet' of activity. Our thinking

on these topics has been influenced by experiments with the '9+2' axoneme of the quail (*Coturnix coturnix*) spermatozoon (Vernon and Woolley, 1995). We split quail axonemes longitudinally using a mechanical, not an enzymatic, method. We then reactivated the groups of doublets by gradually raising the ATP level, observing continuously. (The ATP was released photolytically from caged ATP.) Dynein activity generated tension locally and deformed the geometry of the assembly in a systematic way. Tension generation was not necessarily immediate. When it began, its onset was localised at the proximal end and then propagated, often as a short zone of constant length. This is the experiment that indicates directional mechanical triggering of activity. The 'proximal end' of these preparations was not the natural basal extremity, since the axonemes had been broken off; however, a proximal broken end simulates the natural basal end in that the dyneins here cannot be influenced by any other situated more proximally. (Nevertheless, the natural anchorages in the true basal end augment the excitability in some way; Woolley and Bozkurt, 1995.) A self-organizing control system for propagation involving the mechanical excitation of the dynein by shear strain has been examined theoretically by Murase and Shimizu (Murase and Shimizu, 1986).

(iv) It has commonly been supposed that, in generating a helical wave, each dynein array is activated sequentially. The limited experimental support for this includes the demonstration of rotatory shifting of the bending plane around the axoneme in the neck region of the '9+0' eel (*Anguilla anguilla*) sperm flagellum (Woolley, 1998), and the same phenomenon in the '9+9+2' sperm of passerine birds such as *Sturnus vulgaris* (Vernon and Woolley, 1999). The proposal of refractoriness would guarantee the progression of the circumferential triggering around the basal end of the axoneme. The idea that the cycle mechanically re-initiates itself, indefinitely, is attractive but we cannot reconcile it with the observed pulsatility.

(v) For helical waves, the direction of circumferential propagation was anticlockwise in, for example, *Echinus esculentus* and *Sturnus vulgaris*, clockwise in *Anguilla anguilla* and, as discussed earlier, occurred in either direction in *Ciona intestinalis* (Brokaw, 1966). If circumferential propagation can be triggered in either direction, we suppose that a sufficiently energetic activation in one array might trigger circumferential propagation in both directions simultaneously. Our key suggestion, then, is that unidirectional circumferential propagation generates the helical wave, while bi-directional circumferential propagation generates the planar wave. Our idea that the determining factor should be the non-linear (yielding) behaviour of the nexin links is consistent with the much greater sliding displacements necessary for torsion-free planar bending as compared with helical waves involving torsion (Holwill et al., 1979). Bi-directional, circumferential spread of activity was suggested in the context of contraction theories by Bradfield (Bradfield, 1955).

Some of our earlier observations can be re-interpreted as 'subthreshold' in relation to the strain in the nexin links. In this situation, the effects of sliding will be localised. Localised tension development was seen in the responses of split quail sperm axonemes to having ATP released around them (Vernon and Woolley, 1995). 'Localized tension' seemed incompatible with the sliding microtubule theory. But those doublets had the form of helical ribbons, and we can now see that strain in the nexin links could have remained subthreshold through the distribution of force to the easily deformable helical superstructure. These travelling zones of tension are now seen as equivalent to the activity underlying helical waves. For planar waves, then, our hypothesis is explicitly that spontaneous activation at the base of one array of dyneins (array n) triggers both the adjacent arrays (n+1, n–1), then (n+2, n–2), then (n+3, n–3) and finally (n+4, n–4). Each triggering also establishes a propagation distally along the array. Although refractoriness again gives progressivity and would ensure that the sequence will re-start at array n, there is evidence that local curvature influences excitability (Yeung and Woolley, 1983). Which of the nine doublets initiates the cycle? Gibbons et al. (Gibbons et al., 1987) showed that in sea urchin spermatozoa the plane of beating could be altered by an imposed vibration. From the fact that the axoneme itself remained untwisted (Shingyoji et al., 1991b), it follows that any one of the dynein arrays can act as array n and initiate the activity. However, we think that the pattern of spread normally stabilizes to be symmetrical about an axis parallel to the plane containing the central pair (Bannai et al., 2000). The absence of a central pair may be a factor reducing the likelihood of a planar wave (Ishijima et al., 1988). Bi-directional spread around the base of the axoneme would reproduce the pattern of activation that Wais-Steider and Satir (Wais-Steider and Satir, 1979) deduced must underlie planar bending according to the assumptions of the 'sliding microtubule theory'. This well-established theory, recently discussed by Woolley (Woolley, 2000), is therefore accommodated in a general way in what we propose.

It remains to be explained how the bends come to be stabilized as planar whereas the interbends, according to our results, are susceptible to torsion and tilting. The only study of torsion in sea urchin sperm flagella is that of Gibbons (Gibbons, 1975), who concluded provisionally that torsions occurred only at the conjunctions of inter-bends with bends and that successive torsions (four in each cycle) had alternate chirality. Using this result, we suggest that a bend with oppositely directed torsional stresses at each end will tend to stabilize as planar. However, given that dynein generates force with a single polarity, it is unlikely that torsions can be generated actively with either chirality. It may be that there is some degree of resting sinistral chirality (Vernon, 1996) upon which regions of active dextral chirality are imposed, the net effect being substantial lengths of axoneme without any torsion. Our study of strictly planar waveforms in living quail spermatozoa could detect no torsions at all (Woolley and Vernon, 1999).

(vi) By this theory, raising the external viscosity or reducing the force of active sliding should increase the likelihood of helical

waves. One should expect planar bending to be shown by normally motile cells at low external viscosities, as is true for echinoderm spermatozoa. Helical bending should be inducible at moderate viscosities if the motility is impaired, as demonstrated by Brokaw (Brokaw, 1966) in *Ciona intestinalis*. For normally motile cells, a higher external viscosity will be needed to convert planar to helical bending, as shown in our use of media of 1.5 Pa s. A further complexity, however, seems unavoidable. The reversion from helical to planar bending, seen in *Echinus esculentus* at even higher viscosity (4 Pa s) or when helical sperm encounter an obstruction, must imply a further increase in the active force (unless the stiffness suddenly changes). This proposal of an increment in active force is equivalent to suggesting that these spermatozoa can respond actively to environmental conditions. The response to obstruction is even an 'appropriate' response since the acceleration of the spermatozoa tends to displace the obstruction. In our study of quail spermatozoa moving through highly viscous media, we frequently saw that a spermozoon would swim helically until it happened to stick by its head: then, immediately, a torsion-free plane meander would ensue (Woolley and Vernon, 1999). In retrospect, the onset of the planar waveform in quail spermatozoa is, we suggest, another example of an increment in active force. We have also found that the spermatozoa of *Sturnus vulgaris* change waveform and swim faster when the viscosity is increased (Vernon and Woolley, 1999). One testable conjecture is that shear-sensitive ion channels in the plasma membrane are stimulated. It is well known that the bend angles developed by mammalian spermatozoa increase markedly with an influx of Ca^{2+}, the phenomenon of 'hyperactivation' (for a review, see Suarez, 1996).

Concluding remarks

Many authors, in the early reviews of cytology and in textbooks describing the locomotion of protozoa, have been content to assume that there are just two types of flagellar motion in eukaryotes, planar and helical. According to our findings, this simple view is valid, with a proviso regarding quasi-planarity. The ability of the flagellum to adapt to and even respond to conditions of increased external viscosity is probably related to the ability of the spermatozoon to penetrate the jelly coat around the egg and then exert force strenuously against the vitelline membrane.

This work was supported by a research grant from the Biotechnology and Biological Sciences Research Council (UK). We thank Dr M. E. J. Holwill for valuable advice. Video sequences of some of the phenomenon described can be found at http://www.bris.ac.uk/Depts/Physiology/Staff/DWGroup/dw.html

References

Afzelius, B. A. (1955). The fine structure of the sea urchin spermatozoa as revealed by the electron microscope. *Z. Zellforsch.* **42**, 134–148.

Amos, L. (1991). Negative stain electron microscopy of microtubules and associated motor molecules. *Micron. Microsc. Acta* **22**, 395–403.

Bannai, J., Yoshimura, M., Takahashi, K. and Shingyoji, C. (2000). Calcium regulation of microtubule sliding in reactivated sea urchin sperm flagella. *J. Cell Sci.* **113**, 831–839.

Bozkurt, H. H. and Woolley, D. M. (1993). Morphology of nexin links in relation to interdoublet sliding in the sperm flagellum. *Cell Motil. Cytoskel.* **24**, 109–118.

Bradfield, J. R. G. (1955). Fibre patterns in animal flagella and cilia. *Symp. Soc. Exp. Biol.* **9**, 306–334.

Brokaw, C. J. (1965). Non-sinusoidal bending waves of sperm flagella. *J. Exp. Biol.* **43**, 155–169.

Brokaw, C. J. (1966). Effects of increased viscosity on the movements of some invertebrate spermatozoa. *J. Exp. Biol.* **45**, 113–139.

Brokaw, C. J. (1975). Effects of viscosity and ATP concentration on the movement of reactivated sea-urchin sperm flagella. *J. Exp. Biol.* **62**, 701–719.

Brokaw, C. J. (1988). Bending-wave propagation by microtubules and flagella. *Math. Biosci.* **90**, 247–263.

Brokaw, C. J. (1996). Microtubule sliding, bend initiation and bend propagation parameters of *Ciona* sperm flagella altered by viscous load. *Cell Motil. Cytoskel.* **33**, 6–21.

Buller, A. H. R. (1902). Is chemotaxis a factor in the fertilization of the eggs of animals? *Q. J. Microsc. Sci.* **46**, 145–176.

Chwang, A. T. and Wu, T. Y. (1971). A note on the helical movement of micro-organisms. *Proc. R. Soc. Lond. B* **178**, 327–346.

Gibbons, I. R. (1963). Studies on the protein components of cilia from *Tetrahymena pyriformis*. *Proc. Natl. Acad. Sci. USA* **50**, 1002–1010.

Gibbons, I. R. (1975). The molecular basis of flagellar motility in sea urchin spermatozoa. In *Molecules and Cell Movement* (ed. S. Inoué and R. E. Stephens), pp. 207–232. New York: Raven Press.

Gibbons, I. R. (1982). Sliding and bending in sea urchin sperm flagella. *Symp. Soc. Exp. Biol.* **35**, 225–287.

Gibbons, I. R., Shingyoji, C., Murakami, A. and Takahashi, K. (1987). Spontaneous recovery after experimental manipulation of the plane of beat in sperm flagella. *Nature* **325**, 351–352.

Gray, J. (1955). The movement of sea-urchin spermatozoa. *J. Exp. Biol.* **32**, 775–801.

Hiramoto, Y. and Baba, S. A. (1978). A quantitative analysis of flagellar movement in echinoderm spermatozoa. *J. Exp. Biol.* **76**, 85–104.

Holwill, M. E. J., Cohen, H. J. and Satir, P. (1979). A sliding microtubule model incorporating axonemal twist and compatible with three-dimensional ciliary bending. *J. Exp. Biol.* **78**, 265–280.

Ishijima, S. and Hamaguchi, Y. (1993). Calcium ion regulation of chirality of beating flagellum of reactivated sea urchin spermatozoa. *Biophys. J.* **65**, 1445–1448.

Ishijima, S. and Hiramoto, Y. (1994). Flexural rigidity of echinoderm sperm flagella. *Cell Struct. Funct.* **19**, 349–362.

Ishijima, S., Ishijima, S. I. and Afzelius, B. A. (1994). Movement of *Myzostomum* spermatozoa: calcium ion regulation of swimming direction. *Cell Motil. Cytoskel.* **28**, 135–142.

Ishijima, S., Sekiguchi, K. and Hiramoto, Y. (1988). Comparative study of the beat patterns of American and Asian horseshoe crab sperm: evidence for a role of the central pair complex in forming planar waveforms in flagella. *Cell Motil. Cytoskel.* **9**, 264–270.

Jarosch, R. (1986). The mechanical behaviour of doublet microtubules simulated by helical models. *Cell Motil. Cytoskel.* **6**, 209–261.

Kamiya, R. and Okagaki, T. (1986). Cyclical bending of two outer-doublet microtubules in frayed axonemes of *Chlamydomonas*. *Cell Motil. Cytoskel*. **6**, 580–585.

Minoura, I., Yagi, T. and Kamiya, R. (1999). Direct measurement of inter-doublet elasticity in flagellar axonemes. *Cell Struct. Funct*. **24**, 27–33.

Murase, M. and Shimizu, H. (1986). A model of flagellar movement based on co-operative dynamics of dynein–tubulin cross-bridges. *J. Theor. Biol.* **119**, 409–433.

Rikmenspoel, R. (1978). Movement of sea urchin sperm flagella. *J. Cell Biol*. **76**, 311–322.

Rothschild, Lord and Swann, M. M. (1949). The fertilization reaction in the sea urchin egg. *J. Exp. Biol*. **26**, 164–176.

Shingyoji, C., Gibbons, I. R., Murakami, A. and Takahashi, K. (1991a). Effect of imposed head vibration on the stability and waveform of flagellar beating in sea urchin spermatozoa. *J. Exp. Biol.* **156**, 63–80.

Shingyoji, C., Katada, J., Takahashi, K. and Gibbons, I. R. (1991b). Rotating the plane of imposed vibration can rotate the plane flagellar beating in sea-urchin sperm without twisting the axoneme. *J. Cell Sci.* **98**, 175–181.

Shingyoji, C., Murakami, A. and Takahashi, K. (1977). Local reactivation of Triton-extracted flagella by iontophoretic application of ATP. *Nature* **265**, 269–270.

Silvester, N. R. and Holwill, M. E. J. (1972). An analysis of hypothetical flagellar waveforms. *J. Theor. Biol.* **35**, 505–523.

Sokal, R. R. and Rohlf, F. J. (1995). *Biometry – The Principles and Practice of Statistics in Biological Research*. Third edition. New York: W. H. Freeman.

Suarez, S. S. (1996). Hyperactivated motility in sperm. *J. Androl*. **17**, 331–335.

Takahashi, K., Shingyoji, C. and Kamimura, S. (1982). Microtubule sliding in reactivated flagella. *Symp. Soc. Exp. Biol*. **35**, 159–177.

Vernon, G. G. (1996). Mechanical activity and its propagation along the flagellar axoneme: studies using caged ATP. PhD thesis, Bristol University. 108pp.

Vernon, G. G. and Woolley, D. M. (1995). The propagation of a zone of activation along groups of flagellar doublet microtubules. *Exp. Cell Res.* **220**, 482–494.

Vernon, G. G. and Woolley, D. M. (1999). Three-dimensional motion of avian spermatozoa. *Cell Motil. Cytoskel*. **42**, 149–161.

Wais-Steider, J. and Satir, P. (1979). Effect of vanadate on gill cilia: switching mechanism in ciliary beat. *J. Supramol. Struct*. **11**, 339–347.

Warner, F. D. (1983). Organization of interdoublet links in *Tetrahymena* cilia. *Cell Motil.* **3**, 321–332.

Warner, F. D. and Satir, P. (1974). The structural basis of ciliary bend function. Radial spoke positional changes accompanying microtubule sliding. *J. Cell Biol*. **63**, 35–63.

Woolley, D. M. (1977). Evidence for ‘twisted plane’ undulations in golden hamster sperm tails. *J. Cell Biol*. **75**, 851–865.

Woolley, D. M. (1995). The extrusion of membranous threads by avian and mammalian spermatozoa, *in vitro*. *J. Submicrosc. Cytol. Pathol*. **27**, 281–290.

Woolley, D. M. (1998). Studies on the eel sperm flagellum. 3. Vibratile motility and rotatory bending. *Cell Motil. Cytoskel*. **39**, 246–255.

Woolley, D. M. (2000). The molecular motors of cilia and eukaryotic flagella. *Essays Biochem*. **35**, 103–115.

Woolley, D. M. and Bozkurt, H. H. (1995). The distal sperm flagellum: its potential for motility after separation from the basal structures. *J. Exp. Biol*. **198**, 1469–1481.

Woolley, D. M. and Osborn, I. W. (1984). Three-dimensional geometry of motile hamster spermatozoa. *J. Cell Sci*. **67**, 159–170.

Woolley, D. M. and Vernon, G. G. (1999). Alternating torsions in a living ‘9+2’ flagellum. *Proc. R. Soc. Lond. B* **266**, 1271–1275.

Yeung, C. H. and Woolley, D. M. (1983). A study of bend formation in locally reactivated hamster sperm flagella. *J. Muscle Res. Cell Motil.* **4**, 625–645.